Nano Research

Open Access

Research Article

Living nanoparticle assemblies emergent from predominantly entropic forces

Zongze Zhang[1], Fenghua Zhang[1,3] ✉, Jingjing Wei[1,2], and Zhijie Yang[1] ✉

[1] *Key Laboratory of Colloid and Interface Chemistry, Ministry of Education, School of Chemistry and Chemical Engineering, Shandong University, Jinan 250100, China*
[2] *Shenzhen Research Institute of Shandong University, Shenzhen 518000, China*
[3] *Suzhou Research Institute of Shandong University, Suzhou 215123, China*

Cite this article: *Nano Research*, **2026**, *19*, 94908801. https://doi.org/10.26599/NR.2026.94908801

ABSTRACT: Self-assembly of nanoparticles is typically governed by enthalpic interactions such as van der Waals forces, hydrogen bonding, or ligand-mediated attractions. Here, we show that nanoparticles can spontaneously form dynamic "living" chains—growing, breaking, and reorganizing—predominantly entropy-driven by entropic effects, without specific chemical interactions. Spectroscopic, microscopic, and thermodynamic analyses reveal that the driving force is a substantial entropy gain arising from the displacement of confined solvent molecules inside supramolecular nanotubes, akin to entropy-driven host–guest complexation. This process exhibits features of dynamic equilibrium, including nonlinear fluorescence quenching and continuous exchange of nanoparticles inside and outside the nanotubes. We further demonstrate that assembly efficiency depends on nanoparticle size, solvent chain length, and polarity, and enable *in situ* dynamic replacement of Ag nanoparticles with Au nanoparticles within the nanotubes. These results establish a general entropy-driven strategy for constructing dynamic, ordered nanohybrid materials under mild conditions.

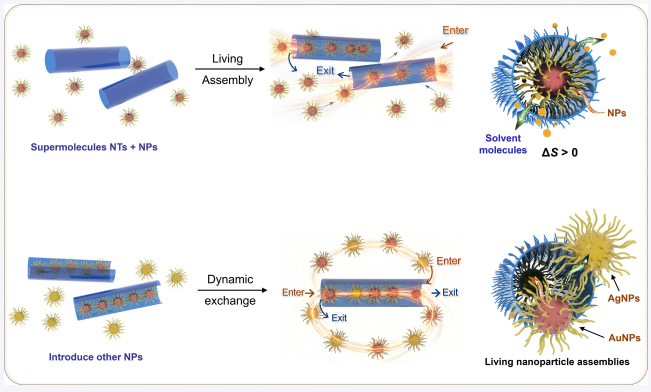

KEYWORDS: self-assembly, entropic effects, supramolecular, nanohybrid material

1 Introduction

The construction of ordered nanoparticle (NP) assemblies, especially in one-dimensional (1D) configurations—such as chains, wires, and fibrillar architectures—represents a frontier in nanoscience due to their unique anisotropic properties and potential applications in electronics, optics, and catalysis [1–7]. However, achieving reversible and tunable 1D assemblies remains challenging with current approaches. Conventional approaches rely on enthalpy-driven interactions—van der Waals forces, hydrogen bonding, or ligand-mediated attractions—often requiring harsh solvents [8–12]. Many current strategies drive NP assembly by increasing system entropy, yet the resulting superstructures are thermodynamically stable and non-living [13–19]. Consequently, exploring alternative driving forces, particularly in mild solvent environments, remains a significant challenge for developing dynamic composites, especially those capable of forming multicomponent structure and reconfigurable 1D nanostructures.

Despite the intrinsic tendency of π-conjugated molecules to form one-dimensional stacks and nanoparticles to adopt three-dimensional packing [20–26], these components can be integrated into co-assemblies under conditions of moderate chemical affinity [27–31]. In previous studies, supramolecular nanotubes (NTs) formed from organic molecules such as perylene diimides (PDIs) have provided one-dimensional channels for arranging metallic nanoparticles into precise architectures [8–10]. Macrocyclic molecules with open cavities have been widely explored as host materials for selectively encapsulating complementary guests [32–37]. The formation of host–guest systems often involves more than one type of non-covalent interaction [38], which is similar to the driving forces behind nanoparticle self-assembly [39]. Nevertheless, this concept has rarely been extended to the co-assembly of nanoparticles within organic nanotubes. In contrast,

Received: March 30, 2026; **Revised:** April 30, 2026
Accepted: April 30, 2026

✉Address correspondence to Fenghua Zhang, zhangfenghua@sdu.edu.cn; Zhijie Yang, zyangchem@sdu.edu.cn

nature frequently harnesses entropy to drive sophisticated self-assembly, from protein folding to the organization of biopolymers [40–43]. Entropy-driven assembly provides a distinct and advantageous pathway for ordered nanocomposite materials with a distinct dynamic or living characteristic [44, 45].

In this work, we demonstrate that entropy alone can drive the encapsulation of nanoparticles into nanotubular structures, even in a solvent where both components are individually well dispersed. Nanoparticles can spontaneously assemble into dynamic "living" chains that continuously grow, break apart, and reorganize, predominantly driven by entropic effects without specific chemical interactions. In this process, confined solvent molecules are displaced into the bulk, generating a substantial entropy gain ($\Delta S > 0$), akin to host–guest complexation. This entropic driving force enables dynamic, reversible exchange of nanoparticles, with assembly efficiency strongly dependent on nanoparticle size and solvent chain length. Our findings reveal an "entropy-driven order" pathway and open important avenues for constructing dynamic, tunable, and environmentally benign nanomaterials.

2 Results and discussion

2.1 Structure and characterization of NPs/NTs assembly

Previous strategies for enthalpy-driven nanoparticle assembly typically rely on direct, attractive interactions between particles. When nanoparticles associate, they form new, more stable assemblies and release energy ($\Delta H < 0$). We propose a novel mechanism centered on solvent entropy. We hypothesize that the interior of the supramolecular nanotube, lined with densely packed $C_{12}H_{25}$ alkyl chains, constitutes a confined, low-entropy environment for solvent molecules. However, during the ordering process inside the nanotube, a large number of solvent molecules or ions originally bound to the ligands are released. These released small molecules gain substantial motional freedom. Alternatively, the ordered arrangement optimizes the spatial distribution between the particles and the nanotube wall, leading to a significant increase in the total entropy of the entire solvent-nanoparticle-nanotube composite system ($\Delta S >> 0$), thereby driving the ordering process. In this scenario, nanoparticles appear to be "passively" pushed together. The driving force originates from the increased entropy of the solvent or small molecules, rather than from direct interparticle attraction, which constitutes the key mechanistic distinction (Fig. 1(a)). More interestingly, structures formed via predominantly entropy-driven assembly are often non-rigid. Because they are stabilized not by strong bonding forces but by an effective "pushing force" from the solvent environment, the resulting architecture is more dynamic. Particles can exchange or adjust within the ordered framework, exhibiting what we term "living assemblies" (Fig. 1(b)).

PDI derivative molecule (PDI-1) was synthesized according to a previous report (Fig. 2(a) and Scheme S1 and Fig. S1 and Methods in the Electronic Supplementary Material (ESM)) [10, 46]. Subsequently, using n-hexane as the nonsolvent, nanotubes were prepared via the solvent-nonsolvent method (Fig. 2(f) and Figs. S2(a) and S2(b) and Methods in the ESM). The inner diameter of the nanotubes was measured to be 6.3 ± 0.2 nm (Fig. 2(c) and Fig. S3 in the ESM). Combined with atomic force microscopy (AFM) images, it was demonstrated that the nanotubes mostly exist as bundled aggregates (Fig. 2(d)). Density-functional theory (DFT) calculations reveal that a relaxed dimer structure of molecule PDI-1 displays an interplanar π–π distance of 3.3 Å and a rotational twist angle of 143° (Fig. 2(b)), suggesting the formation of J-type helical stacks upon their assembly (Fig. S4 in the ESM). Meanwhile, we synthesized a series of dodecanethiol (DDT)-coated AuNPs of varying sizes (Fig. S5 in the ESM). These thiol-coated AuNPs can be well dispersed in alkanes and do not spontaneously form ordered aggregates (Fig. 1(c) and Fig. S6 in the ESM). Under these conditions, the interactions between AuNPs are weaker than the interactions between AuNPs and the solvent, preventing the spontaneous formation of assemblies (Fig. 1(d)). Surprisingly, when nanotubes and an appropriate amount of AuNPs were co-dispersed in n-hexane, the AuNPs—which originally remained well-dispersed in n-hexane—entered the PDI nanotubes and assembled into one-dimensional ordered arrays (Fig. 1(e)). At this point, the nanoparticles are in a good solvent and spontaneously assemble into a one-dimensional ordered structure, indicating that entropy change plays a crucial role in this process (Fig. 1(f)). High-resolution electron microscopy observations revealed that the AuNPs are arranged in an one-dimensional, long-range ordered pattern inside the nanotubes. Within each nanotube, the AuNPs align in a single chain (Fig. 2(e) and Fig. S7 in the ESM). Combined SEM images demonstrate that nanoparticles are assembled within the supramolecular nanotubes (Fig. S8 in the ESM). Due to the fluorescent emission of supramolecular nanotubes, we observed their fluorescence *in situ* using fluorescence optical microscopy. Over time, the fluorescence of the supramolecular nanotubes gradually quenched (Fig. S9 in the ESM). During the one-dimensional assembly process, the intensity of the ultraviolet–visible (UV–vis) spectra peak of the residual AuNPs in solution gradually decreased over time (Fig. 2(g)), indicating a continuous reduction in the concentration of free AuNPs in solution and a corresponding increase in the filling density of nanoparticles within the nanotubes (Fig. 2(h)). We hypothesize that the formation of this AuNPs/NTs assembly is driven by a novel assembly mechanism.

2.2 Predominantly entropy-driven living NPs/NTs assemblies

In conventional strategies for constructing NPs/NTs co-assemblies, the introduction of alcohol solvents as nonsolvent is typically required. This enhances interactions between particles as well as between particles and nanotubes, thereby promoting the formation of ordered structures. In such nonsolvent mediated assembly processes, the enthalpy change of the system plays a dominant role, and the reduction in Gibbs free energy primarily relies on the enthalpy contribution. For comparison, the co-assembly of the PDI-1 molecule with AuNPs was conducted in a nonsolvent (ethanol), which led to enthalpy-driven formation of assemblies similar to those described above, with nanoparticles arranged one-dimensionally within supramolecular nanotubes (Figs. 2(i)–2(k) and Fig. S10 in the ESM). However, when the ratio between the two components was imbalanced, i.e., with an excess of nanoparticles, the surplus nanoparticles aggregated outside the nanotubes, forming a separate phase (Fig. S11 in the ESM). When nanoparticle quantities are extremely low, the particle distribution states of enthalpy-driven assemblies and entropy-driven assemblies exhibit significant differences. Particles in enthalpy-driven assemblies tend to aggregate in multiple clusters, whereas nanoparticles in entropy-driven assemblies remain relatively dispersed (Fig. S12 in the ESM).

The PDIs molecules exhibit excellent fluorescence properties,

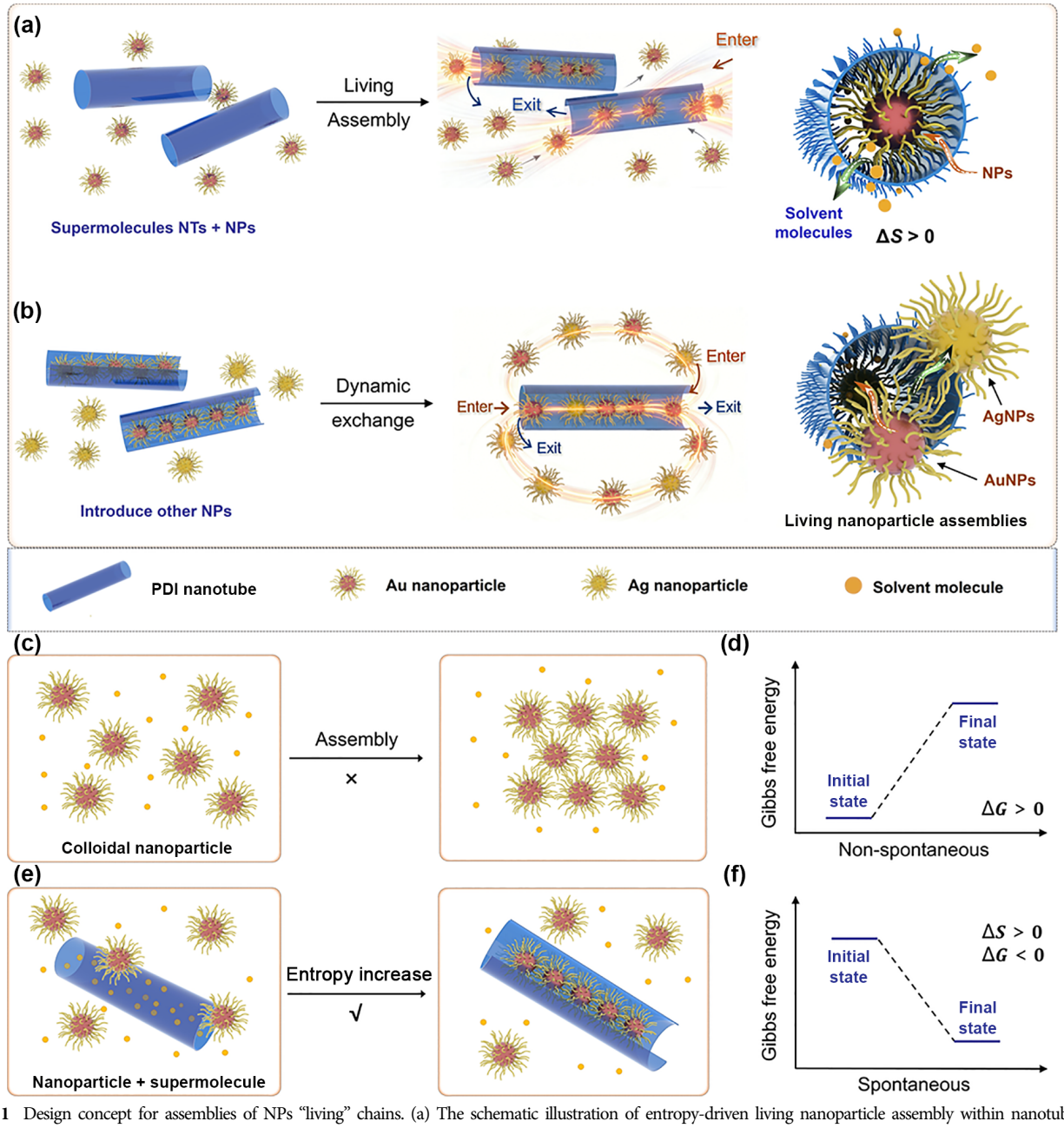

Figure 1 Design concept for assemblies of NPs "living" chains. (a) The schematic illustration of entropy-driven living nanoparticle assembly within nanotubes. (b) Dynamic exchange and positional adjustment of nanoparticles inside nanotubes. (c) Schematic diagram of colloidal nanoparticle self-assembly in good solvent. (d) Energy change of colloidal nanoparticle self-assembly in good solvent. (e) Schematic diagram of colloidal nanoparticle assembly in good solvent with nanotubes. (f) Energy change of colloidal nanoparticle self-assembly in good solvent with nanotubes.

and within the co-assembled system, the AuNPs serve as the exclusive fluorescence quenchers, capable of quenching the fluorescence emitted by the supramolecular nanotubes. We measured the fluorescence emission peak intensities for different systems across a series of AuNPs concentrations and performed fitting using the Stern–Volmer equation (Figs. 3(a) and 3(b) and Fig. S13 in the ESM). The fluorescence quenching fitting results for the composite assemblies formed by ethanol-driven assembly showed a linear trend (Figs. 3(e) and 3(f)), whereas the fluorescence quenching of supramolecular nanotubes by AuNPs co-assembled in n-hexane exhibited a nonlinear pattern (Figs. 3(c) and 3(d)). This indicates that the former fluorescence quenching system follows a single quenching mechanism, while the latter involves at least two distinct fluorescence quenching mechanisms. The nonlinear curve fits the Stern–Volmer equation of the mixed quenching model, demonstrating the simultaneous presence of both static and dynamic quenching mechanisms [47, 48]. When we isolated the assemblies from the solution and tested them by spot-drying onto quartz plates, the fluorescence quenching fit transitioned from nonlinear to linear (Figs. S14 and S15 in the ESM). In the enthalpy-driven co-assembly process in the presence of ethanol, the interaction between AuNPs and supramolecular nanotubes is relatively tight, driven by van der Waals forces and solvophobic interactions, resulting in fixed positions of AuNPs within the nanotubes. In contrast, in the assembly system solely in the presence of n-hexane, the AuNPs are entirely surrounded by a good

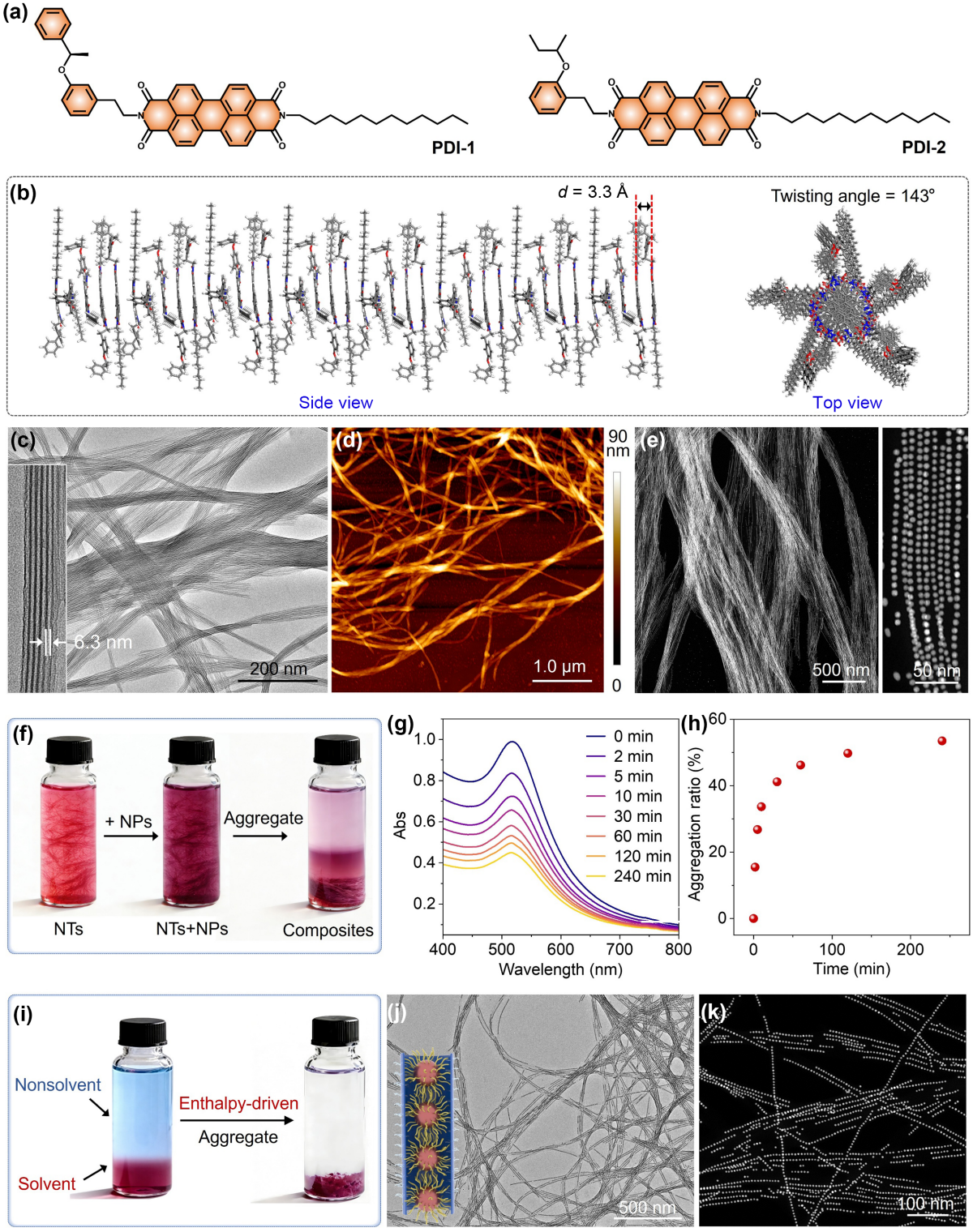

Figure 2 Comparison of entropy-driven and enthalpy-driven of NPs/NTs co-assemblies. (a) Molecular structure of PDI-1 and PDI-2. (b) Molecular stacking model of PDI-1. (c) TEM image of PDI-1 supramolecular nanotubes. (d) AFM image of PDI-1 supramolecular nanotubes. (e) HRTEM-HAADF image of NPs/NTs co assemblies. (f) Schematic diagram of the experimental living assembly process. (g) UV–vis spectra during assembly process. (h) Conversion of nanoparticles entering nanotubes within the system. (i) Schematic diagram of the experimental enthalpy-driven assembly process. (j) TEM image of NPs/NTs enthalpy-driven co-assemblies. The inset is corresponding structural model. (j) HADDF image of NPs/NTs enthalpy-driven co-assemblies.

solvent environment. Consequently, the binding between AuNPs and nanotubes during assembly is weaker, and the assembly process remains in a state of dynamic equilibrium. The AuNPs continuously move within the supramolecular nanotubes, leading to a nonlinear fluorescence quenching fitting curve. Therefore, we propose that in the environment of n-hexane, where nanoparticles are entirely surrounded by a good solvent, the spontaneous assembly of AuNPs within supramolecular nanotubes is driven by

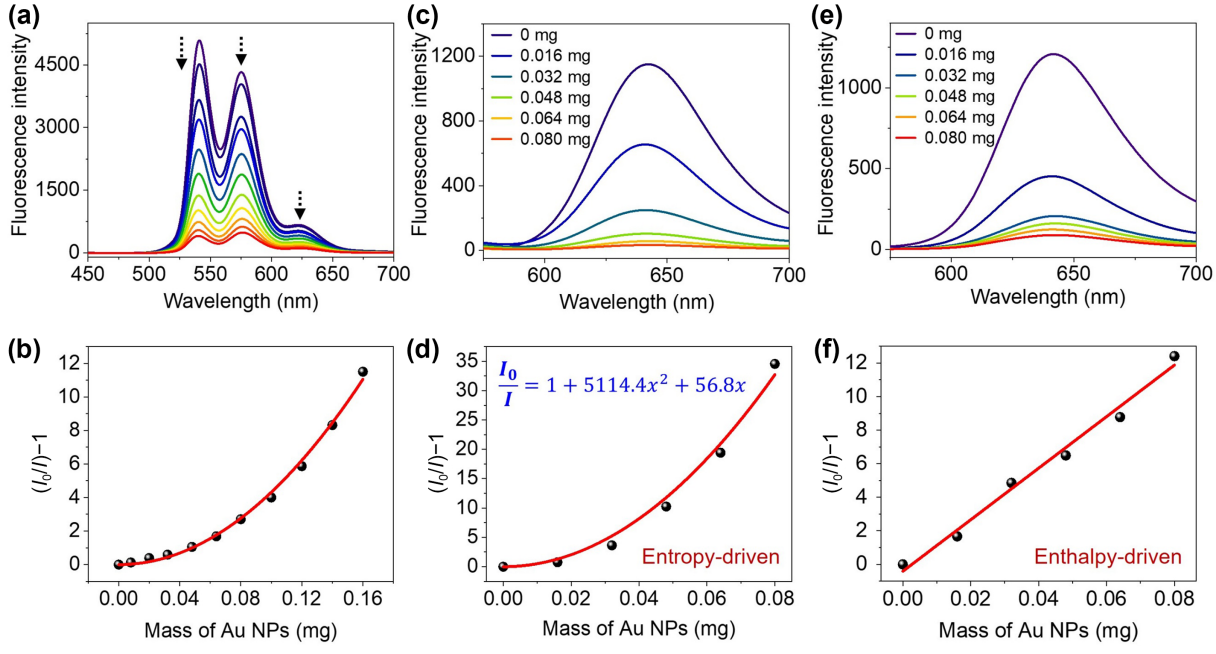

Figure 3 Fluorescence characterizations of entropy-driven and enthalpy-driven of NPs/NTs co-assemblies. Fluorescence spectra of PDI-1 monomer (a) and the Stern–Volmer fitting of fluorescence peak intensity of monomers at different AuNPs concentrations (b). Entropy-driven co-assemblies at different mass of nanoparticles (c), and the corresponding Stern–Volmer fitting of fluorescence peak intensity (d). Enthalpy-driven co-assemblies at different mass of nanoparticles (e), and the corresponding Stern-Volmer fitting of fluorescence peak intensity (f).

the entropy change of the system, resulting in a dynamic equilibrium assembly process. This represents a mechanism for NPs/NTs co-assembly that is entirely distinct from any previously reported mechanisms.

Based on the above hypothesis, we propose the following model: The supramolecular nanotubes are formed by the helical stacking of organic molecules, with their inner walls densely packed with $C_{12}H_{25}$ alkyl chains. The negative curvature of the inner nanotube walls leads to a higher density of these alkyl chains (Fig. S16 in the ESM). In this scenario, the alkane molecules within the nanotubes are constrained by the high-density alkyl chains, resulting in restricted rotational, translational, and conformational entropy of the solvent molecules. Consequently, the system exists in a low-entropy state [49–52]

$$S_{\text{conf}} = k_{\text{B}}\left(N\ln Z - \frac{3}{2}\ln N - \frac{3R^2}{2Na^2}\right) \quad (1)$$

$$S_{\text{trans}} = k_{\text{B}}\ln\left(\frac{e^{5/2}V}{N_{\text{A}}\lambda^3}\right) \quad (2)$$

$$S_{\text{rot}} = -k_{\text{B}}\sum_{i=1}^{M}P_i\ln P_i = -k_{\text{B}}\sum_{i=1}^{M}\frac{1}{M}\ln\frac{1}{M} = k_{\text{B}}\ln M \quad (3)$$

Here, k_{B} is the Boltzmann constant, N represents the number of molecules involved in the assembly process, Z is the coordination number describing the possible neighboring interactions, R and a represent the characteristic molecular size and the average intermolecular spacing, respectively. In the translational entropy term, V denotes the accessible volume of the system, N_{A} is Avogadro's constant, and λ represents the thermal de Broglie wavelength. In the rotational entropy expression, P_i is the probability of the i^{th} orientation state and M represents the number of available molecular orientations. Where, the conformational entropy (S_{conf}) of solvent molecules is closely related to molecular flexibility and carbon chain length (see Eq. (1)). The translational entropy (S_{trans}) is associated with the free space available in the molecular environment (see Eq. (2)). The rotational entropy (S_{rot}) depends on the constraints on molecular orientation in the surrounding space (see Eq. (3)). Since thiol ligands are covalently bound to the surface of nanoparticles, their rotational, translational, and conformational entropy remains in a low-entropy state. When nanoparticles are introduced into the organic nanotube system, the previously confined solvent molecules can be displaced by the nanoparticles and released into the free space of the bulk solvent (see Fig. 1(e)). For covalently bound ligand molecules, the associated entropy loss is relatively small, while the solvent molecules released into the free space gain significant free volume, leading to a substantial entropy increase and a concomitant reduction in free energy for the entire system. Therefore, the driving force for this co-assembly is essentially the entropy increase resulting from the transition of a large number of solvent molecules from confined spaces to free spaces, which drives the formation of locally ordered nanoparticle structures. This is a dynamic process where entropy induces order.

2.3 Effects of nanoparticle size, solvent chain length, and polarity

To validate the correctness of the proposed model, we conducted co-assembly experiments using a series of AuNPs of varying sizes with organic nanotubes (Fig. S17 in the ESM). The experimental results show that as the nanoparticle size increases from 3.0 to 7.1 nm, the filling degree of nanoparticles within the nanotubes initially rises and then declines, reaching its peak when the nanoparticle size is approximately 5.6 nm (Fig. 4(a)). The phenomenon is attributed to the close conformity between the outer curvature of the nanoparticles (5–6 nm in diameter) and the inner curvature of the

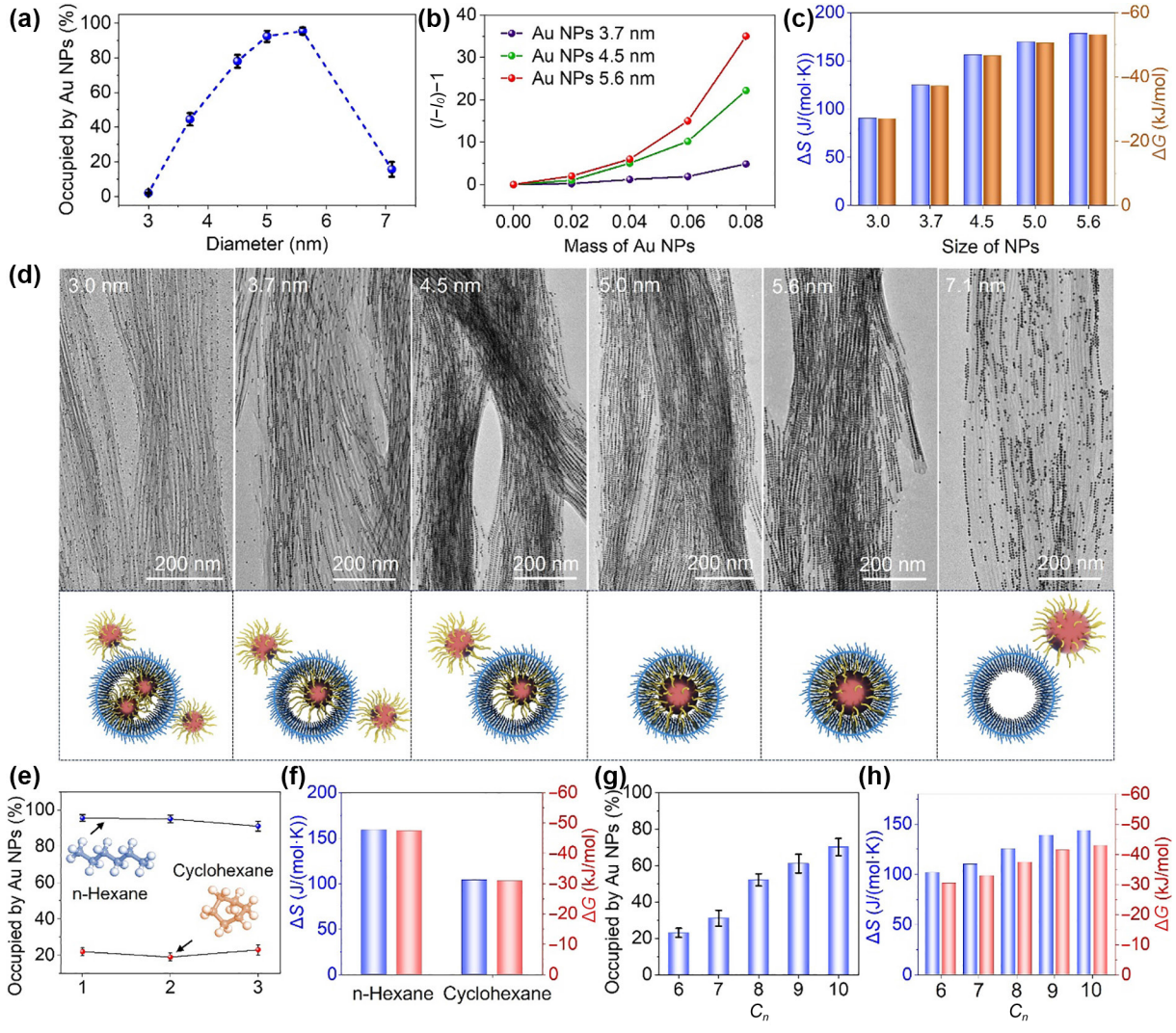

Figure 4 The effect of entropy on NPs/NTs co-assemblies. (a) Packing density of nanoparticles with different sizes in nanotubes. (b) Stern–Volmer fitting of fluorescence peak intensity of enthalpy-driven co-assemblies at different sizes of nanoparticles, and corresponding ΔS and ΔG (c). (d) TEM images of NPs/NTs co assemblies with different sizes of nanoparticles and the insets are corresponding structural models. (e) Based on three repeated experiments, the filling degree of nanoparticles in nanotubes in two different solvents were statistically analyzed, and corresponding ΔS and ΔG (f). (g) Packing density of nanoparticles with different carbon chain lengths of solvent in nanotubes, and corresponding ΔS and ΔG (h).

6.3 nm nanotubes. At this size, the ligands on the nanoparticle surface can fully interact with the alkyl chains on the inner nanotube wall, occupy the tubular space, and displace solvent molecules, while simultaneously avoiding significant steric repulsion (Fig. 4(d)). This configuration provides the greatest free energy change for the system (Fig. 4(c)). Under these conditions, the fluorescence quenching fitting curve remains nonlinear, indicating that the nanoparticles remain in a dynamic state (Fig. 4(b)).

When the solvent was changed from n-hexane to cyclohexane, the filling degree of nanoparticles within the supramolecular nanotubes dropped sharply from approximately 90% to about 20%, based on three repeated experiments (Figs. 4(e) and 4(f) and Figs. S18 and S19 in the ESM). This is attributed to the linear structure of n-hexane, which contributes greater translational and rotational entropy. In the n-hexane system, the nanoparticles exhibited better assembly and a higher filling degree. To further investigate the influence of solvents with different alkyl chain lengths on nanoparticle assembly, we conducted assembly experiments using straight-chain alkanes with carbon chain lengths of C6, C7, C8, C9, and C10 as solvents, while employing supramolecular (PDI-2) nanotubes (Fig. S21 in the ESM) [7] with an inner diameter of 15 nm and AuNPs of 7 nm in size. The experimental results demonstrate that as the alkyl chain length increases, the rotational, translational, and conformational entropy of the solvent molecules also rise. Consequently, the driving force becomes stronger when these molecules are released into free space, leading to a corresponding increase in the filling degree of nanoparticles within the supramolecular nanotubes (Figs. 4(g) and 4(h) and Figs. S20 and S21 in the ESM). We performed co-assembly of nanoparticles with PDI-2 nanotubes in n-hexane at varying concentrations. As the proportion of nanoparticles increases, their packing density within the nanotubes gradually rises. Even when the nanoparticle proportion becomes excessive, no aggregation occurs on the outer walls of the nanotubes; instead, the excess nanoparticles remain dispersed as individual particles in the solvent. This behavior shows a marked contrast to the outcomes typically observed in enthalpy-driven assembly processes (Fig. S22 in the ESM). Based on this,

kinetic and thermodynamic model for the assembly process was constructed as following

$$C_{free} + C_{tube} \rightleftharpoons C_{nps} + C_{sol} \quad (4)$$

$$K = \frac{C_{nps} \times C_s}{C_i \times C_t} \quad (5)$$

$$\Delta G = -RT\ln K = \Delta H - T\Delta S \approx -T\Delta S \quad (6)$$

$$\Delta S = R\ln K \quad (7)$$

where, C_{free} represents the molar concentration of free nanoparticles in the system. C_{tube} represents the molar concentration of sites within the supramolecular nanotube that can be occupied by nanoparticles. C_{nps} represents the molar concentration of nanoparticles within the supramolecular nanotubes. C_{sol} represents the molar concentration of the displaced solvent molecules. Based on the assembly behavior, we established a displacement equilibrium model described by the Eq. (4). The equilibrium constant can be expressed as Eq. (5). Since the nanoparticle assembly process occurs entirely within a single good solvent (n-hexane) and the interactions are exclusively van der Waals forces between alkyl chains, the enthalpy change during this assembly process can be neglected (see Eq. (6)), and the entropy change of the system can be derived (see Eq. (7)).

Firstly, we obtained the corresponding standard curves by measuring the UV–vis absorption spectra of AgNPs/AuNPs at different concentrations (Figs. S23 and S24 in the ESM). Based on this, in this model, the concentrations of nanoparticles added to the system and the concentrations of free nanoparticles after the system reached assembly equilibrium were determined using UV–vis absorption spectra. We investigated living assembly systems under varying AuNPs/AgNPs addition concentrations. We calculated nanoparticle concentrations within the system using concentration-absorbance calibration curves and estimated the concentration of vacant sites within the supramolecular nanotubes based on the total particle capacity (Figs. 5(a) and 5(c)). Theoretically, for particles of the same type, the Gibbs free energy change and entropy change should be identical at different particle addition concentrations. Combining the thermodynamic model of assembly, the overall entropy changes and Gibbs free energy change of the assembly system at different concentrations were calculated. The entropy change for the AuNPs co-assembly system was found to be 178.4 J/(mol·K) (Fig. 5(b)), while that for the AgNPs co-assembly system was 128.8 J/(mol·K) (Fig. 5(d)).

2.4 *In situ* dynamic replacement of nanoparticles within the nanotubes

Based on the above conclusion, since the nanoparticles within the nanotubes are in a state of dynamic equilibrium, it is possible that free nanoparticles outside the nanotubes undergo dynamic exchange with the ordered nanoparticles inside the nanotubes. Compared to the AgNPs/NTs co-assembly, the AuNPs/NTs co-assembly process exhibits a larger entropy change (Figs. 5(a)–5(d)), indicating stronger binding affinity between AuNPs and nanotubes. Therefore, when the AgNPs/NTs co-assemblies were dispersed in a n-hexane solution containing AuNPs, the AgNPs were gradually displaced outside the nanotubes, while AuNPs continuously entered the nanotubes (Fig. 1(b)). Over a 10-hour monitoring period, the concentration of free AgNPs outside the nanotubes progressively increased (Figs. 5(e) and 5(f)) and the percentage of AuNPs progressively increased (Fig. S25 in the ESM). We fitted the kinetics of the particle replacement process and found that it does not follow conventional reaction kinetics equations. We attribute this to the influence of the rate-limiting step in the kinetics. During assembly, constrained by the flux limitation at the ends of the supramolecular nanotubes, the rate-limiting step is the passage of nanoparticles through the gate into the tube. Under these conditions, the displacement reaction between AuNPs or AgNPs is affected by multiple factors, including the flux at the tube ends and the displaced particles, causing the kinetic rate constant to continuously change. Simultaneously, HRTEM-high angle annular dark field (HAADF) images revealed that both AuNPs and AgNPs were co-assembled in an ordered manner within the nanotubes (Fig. 5(g) and Fig. S26 in the ESM). Grayscale intensity profiles further confirmed that the one-dimensional AgNPs chain-like assemblies were interspersed with AuNPs (Fig. 5(h)). These experimental results further demonstrate that the nanoparticles in the assemblies are in a state of dynamic equilibrium, with continuous movement and exchange occurring between nanoparticles inside and oustside the nanotubes. Elemental oxygen analysis confirmed that after the exchange between the two types of nanoparticles reached equilibrium, the nanotubes exhibited an interspersed distribution of these two nanoparticles (Fig. 5(i)).

3 Conclusion

This study introduces a new strategy in which nanoparticles can spontaneously assemble into dynamic "living" chains. Driven predominantly by entropic effects without specific chemical interactions, these chains continuously grow, break apart, and reorganize. The assembly is caused by the significant entropy increase when AuNPs displace confined solvent molecules inside the nanotubes, leading to a dynamic equilibrium. This is confirmed by nonlinear fluorescence quenching, size-dependent assembly, and spontaneous exchange between AuNPs and AgNPs. Thermodynamic measurements show a substantial entropy gain (ΔS = 178.4 J/(mol·K)) for AuNPs, highlighting an "entropy-driven order" pathway. This mechanism offers a versatile, mild-condition method for creating dynamic nanohybrid materials. A deeper theoretical understanding will further enhance control over these dynamic architectures.

Electronic Supplementary Material: Supplementary material (experimental design including materials, synthesis of nanoparticle and molecules, self-assembly of nanotubes and nanocomposites, characterization techniques and supplementary figures) is available in the online version of this article at https://doi.org/10.26599/NR.2026.94908801.

Data availability

All data that support this work are available within the paper and its Electronic Supplementary Material. Source data are provided in the paper.

Acknowledgements

This work was financially supported by the National Natural

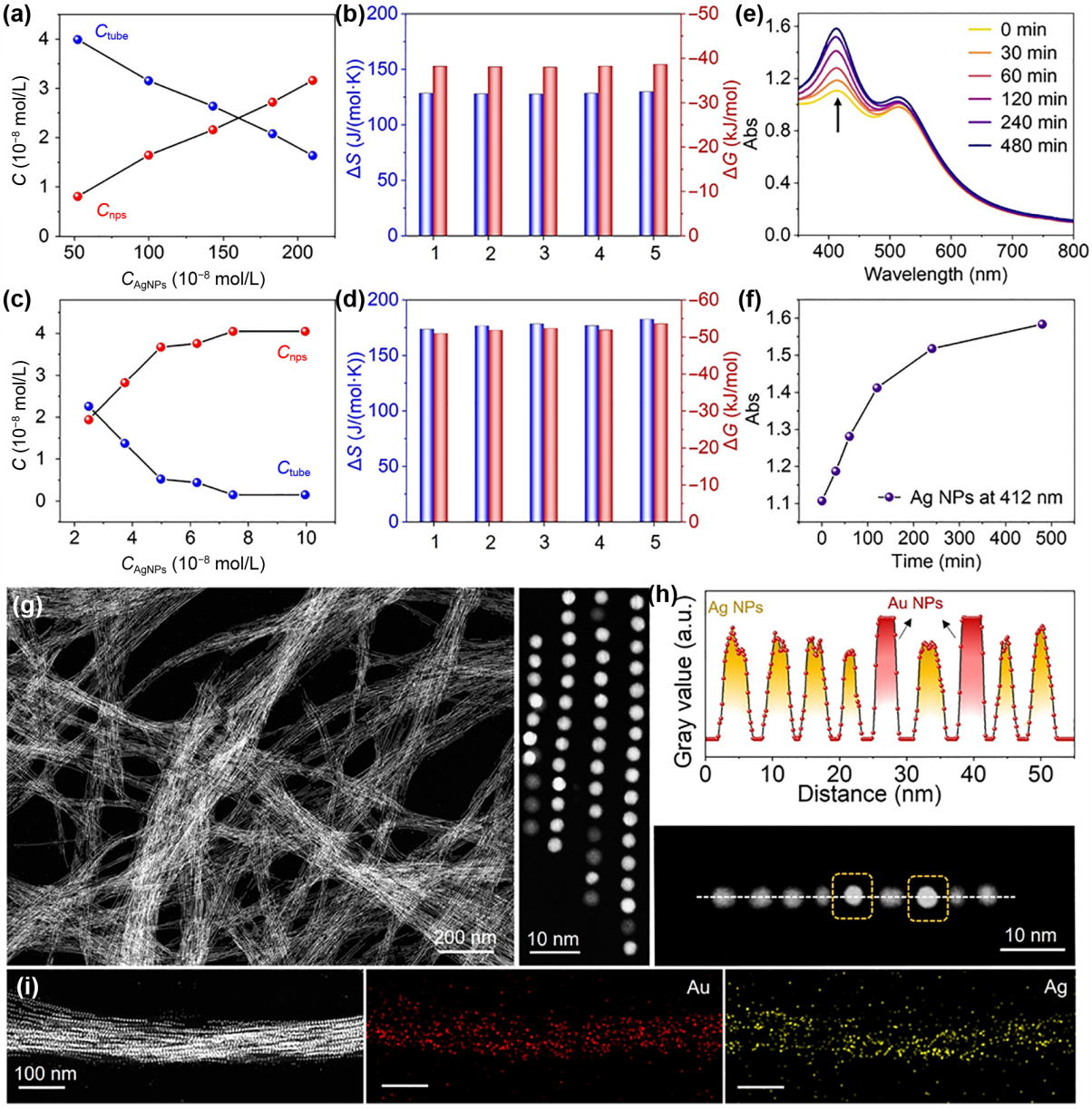

Figure 5 Dynamic exchange of nanoparticles. (a) AgNPs concentration inside the nanotubes of co-assemblies at different concentrations. (b) Entropy changes and Gibbs free energy change in AgNPs/NTs co-assembly systems at different concentrations. (c) AuNPs concentration inside the nanotubes of co-assemblies at different concentrations. (d) Entropy changes and Gibbs free energy change in AuNPs/NTs co-assembly systems at different concentrations. (e) UV–vis spectra of dynamic exchange processes of AuNPs and AgNPs. (f) Decreases of absorption during the excretion of AgNPs. (g) HRTEM-HAADF images of AuNPs/AgNPs/NTs co-assemblies. (h) Randomly arranged AuNPs and AgNPs within nanotubes. (i) HRTEM-mapping images of AuNPs/AgNPs/NTs co-assemblies. The scale bars are 100 nm.

Science Foundation of China (No. 22372089), Guangdong Basic and Applied Basic Research Foundation (No. 2024A1515030066), Taishan Scholar of Shandong Province (Nos. tsqn202408063 and tsqn202408160), and Project of Jinan Bureau of Science and Technology (No. 202333048).

Declaration of competing interest

The authors declare no competing financial interest.

Author contribution statement

The manuscript was written through contributions of all authors. Z. Z. Z.: Designed and conducted the experiments, organized the data, and wrote the manuscript. F. H. Z.: Guided the experiments, organized the data, managed the project, and wrote the manuscript. J. J. W.: Guided the experiments, managed the project, secured funding, and wrote the manuscript. Z. J. Y.: Guided the experiments, managed the project, secured funding, and wrote the manuscript. All authors approved the final manuscript.

Use of AI statement

None.

References

[1] Yao, Y.; Chaubey, G. S.; Wiley, J. B. Fabrication of nanopeapods:

Scrolling of niobate nanosheets for magnetic nanoparticle chain encapsulation. *J. Am. Chem. Soc.* **2012**, *134*, 2450–2452.

[2] Yang, X. S.; Liu, T. H.; Li, R. M.; Yang, X. X.; Lyu, M.; Fang, L.; Zhang, L.; Wang, K.; Zhu, A. Q.; Zhang, L. Y. et al. Host–guest molecular interaction enabled separation of large-diameter semiconducting single-walled carbon nanotubes. *J. Am. Chem. Soc.* **2021**, *143*, 10120–10130.

[3] Jiang, L. X.; de Folter, J. W. J.; Huang, J. B.; Philipse, A. P.; Kegel, W. K.; Petukhov, A. V. Helical colloidal sphere structures through thermo-reversible co-assembly with molecular microtubes. *Angew. Chem., Int. Ed.* **2013**, *52*, 3364–3368.

[4] Li, T. T.; Xue, B.; Wang, B. W.; Guo, G. N.; Han, D. D.; Yan, Y. C.; Dong, A. G. Tubular monolayer superlattices of hollow Mn_3O_4 nanocrystals and their oxygen reduction activity. *J. Am. Chem. Soc.* **2017**, *139*, 12133–12136.

[5] Zhang, F. H.; Liu, R. J.; Wei, Y. Z.; Wei, J. J.; Yang, Z. J. Self-assembled open porous nanoparticle superstructures. *J. Am. Chem. Soc.* **2021**, *143*, 11662–11669.

[6] Wei, Y. Z.; Zhang, F. H.; Wei, J. J.; Yang, Z. J. CdSe 1D/2D mixed-dimensional heterostructures: Curvature-complementary self-assembly for enhanced visible-light photocatalysis. *Small* **2021**, *17*, 2102047.

[7] Wan, S. Y.; Xi, X. Y.; Zhang, H. Y.; Ning, J.; Zheng, Z. Y.; Zhang, Z. B.; Long, Y.; Deng, Y. W.; Fan, P. S.; Yang, D. et al. Shape-mediated oriented assembly of concave nanoparticles under cylindrical confinement. *ACS Nano* **2022**, *16*, 21315–21323.

[8] Bi, Y. T.; Cheng, C. K.; Zhang, Z. Z.; Liu, R. J.; Wei, J. J.; Yang, Z. J. Controlled hierarchical self-assembly of nanoparticles and chiral molecules into tubular nanocomposites. *J. Am. Chem. Soc.* **2023**, *145*, 8529–8539.

[9] Liu, J. M.; Liu, R. J.; Li, H.; Zhang, F. H.; Yao, Q. Y.; Wei, J. J.; Yang, Z. J. Diversifying nanoparticle superstructures and functions enabled by translative templating from supramolecular polymerization. *Angew. Chem., Int. Ed.* **2022**, *61*, e202201426.

[10] Gong, Y. J.; Cao, Z. Z.; Zhang, Z. Z.; Liu, R. J.; Zhang, F. H.; Wei, J. J.; Yang, Z. J. Chirality inversion in self-assembled nanocomposites directed by curvature-mediated interactions. *Angew. Chem., Int. Ed.* **2022**, *61*, e202117406.

[11] Bassani, C. L.; van Anders, G.; Banin, U.; Baranov, D.; Chen, Q.; Dijkstra, M.; Dimitriyev, M. S.; Efrati, E.; Faraudo, J.; Gang, O. et al. Nanocrystal assemblies: Current advances and open problems. *ACS Nano* **2024**, *18*, 14791–14840.

[12] Lee, S.; Sim, K.; Moon, S. Y.; Choi, J.; Jeon, Y.; Nam, J. M.; Park, S. J. Controlled assembly of plasmonic nanoparticles: From static to dynamic nanostructures. *Adv. Mater.* **2021**, *33*, 2007668.

[13] Wan, S. Y.; Xia, X. Y.; Gao, Y. T.; Zhang, H. Y.; Zhang, Z. B.; Wu, F. Y.; Wu, X. S.; Yang, D.; Li, T. T.; Li, J. F. et al. Curvature-guided depletion stabilizes Kagome superlattices of nanocrystals. *Science* **2025**, *387*, 978–984.

[14] Wu, X. S.; Gao, Y. T.; Wang, H.; Zhang, Z. B.; Xi, X. Y.; Yang, D.; Li, T. T.; Dong, A. G. Hydrophobized metal-organic frameworks as versatile building blocks for tailored nanocrystal superlattices. *J. Am. Chem. Soc.* **2025**, *147*, 6361–6366.

[15] Marino, E.; Jiang, Z. Q.; Kodger, T. E.; Murray, C. B.; Schall, P. Controlled assembly of CdSe nanoplatelet thin films and nanowires. *Langmuir* **2023**, *39*, 12533–12540.

[16] Xu, M.; Ku, K. H.; Lee, Y. J.; Shin, J. J.; Kim, E. J.; Jang, S. G.; Yun, H.; Kim, B. J. Entropy-driven assembly of nanoparticles within emulsion-evaporative block copolymer particles: Crusted, seeded, and alternate-layered onions. *Chem. Mater.* **2020**, *32*, 7036–7043.

[17] Zhang, X. F.; Lv, L. F.; Ji, L.; Guo, G. N.; Liu, L. M.; Han, D. D.; Wang, B. W.; Tu, Y. Q.; Hu, J. H.; Yang, D. et al. Self-assembly of one-dimensional nanocrystal superlattice chains mediated by molecular clusters. *J. Am. Chem. Soc.* **2016**, *138*, 3290–3293.

[18] Bian, T.; Gardin, A.; Gemen, J.; Houben, L.; Perego, C.; Lee, B.; Elad, N.; Chu, Z. L.; Pavan, G. M.; Klajn, R. Electrostatic co-assembly of nanoparticles with oppositely charged small molecules into static and dynamic superstructures. *Nat. Chem.* **2021**, *13*, 940–949.

[19] Yao, G. B.; Li, J.; Li, Q.; Chen, X. L.; Liu, X. G.; Wang, F.; Qu, Z. B.; Ge, Z. L.; Narayanan, R. P.; Williams, D. et al. Programming nanoparticle valence bonds with single-stranded DNA encoders. *Nat. Mater.* **2020**, *19*, 781–788.

[20] Hoeben, F. J. M.; Jonkheijm, P.; Meijer, E. W.; Schenning, A. P. H. J. About supramolecular assemblies of π-conjugated systems. *Chem. Rev.* **2005**, *105*, 1491–1546.

[21] Goubet, N.; Portalès, H.; Yan, C.; Arfaoui, I.; Albouy, P. A.; Mermet, A.; Pileni, M. P. Simultaneous growths of gold colloidal crystals. *J. Am. Chem. Soc.* **2012**, *134*, 3714–3719.

[22] Lee, M. S.; Yee, D. W.; Ye, M.; Macfarlane, R. J. Nanoparticle assembly as a materials development tool. *J. Am. Chem. Soc.* **2022**, *144*, 3330–3346.

[23] Li, Z. W.; Fan, Q. S.; Yin, Y. D. Colloidal self-assembly approaches to smart nanostructured materials. *Chem. Rev.* **2022**, *122*, 4976–5067.

[24] Liu, N.; Gao, R. T.; Wu, Z. Q. Helix-induced asymmetric self-assembly of π-conjugated block copolymers: From controlled syntheses to distinct properties. *Acc. Chem. Res.* **2023**, *56*, 2954–2967.

[25] Cheng, Q. H.; Hao, A. Y.; Xing, P. Y. Engineering π-conjugation of phenylalanine derivatives for controllable chiral folding and self-assemblies. *ACS Nano* **2024**, *18*, 5766–5777.

[26] Yao, Z. F.; Cordova, D. L. M.; Milligan, G. M.; Lopez, D.; Allison, S. J.; Kuang, Y. Y.; Ardoña, H. A. M.; Arguilla, M. Q. Lattice-guided assembly of optoelectronically active π-conjugated peptides on 1D van der Waals single crystals. *Sci. Adv.* **2024**, *10*, eadl2402.

[27] Kumar, V. R. R.; Sajini, V.; Sreeprasad, T. S.; Praveen, V. K.; Ajayaghosh, A.; Pradeep, T. Probing the initial stages of molecular organization of oligo(p-phenylenevinylene) assemblies with monolayer protected gold nanoparticles. *Chem. Asian J.* **2009**, *4*, 840–848.

[28] Kao, J.; Xu, T. Nanoparticle assemblies in supramolecular nanocomposite thin films: Concentration dependence. *J. Am. Chem. Soc.* **2015**, *137*, 6356–6365.

[29] Armao, J. J.; Nyrkova, I.; Fuks, G.; Osypenko, A.; Maaloum, M.; Moulin, E.; Arenal, R.; Gavat, O.; Semenov, A.; Giuseppone, N. Anisotropic self-assembly of supramolecular polymers and plasmonic nanoparticles at the liquid-liquid interface. *J. Am. Chem. Soc.* **2017**, *139*, 2345–2350.

[30] Coelho, J. P.; Mayoral, M. J.; Camacho, L.; Martín-Romero, M. T.; Tardajos, G.; López-Montero, I.; Sanz, E.; Ávila-Brande, D.; Giner-Casares, J. J.; Fernández, G. et al. Mechanosensitive gold colloidal membranes mediated by supramolecular interfacial self-assembly. *J. Am. Chem. Soc.* **2017**, *139*, 1120–1128.

[31] Huo, S. W.; Duan, P. F.; Jiao, T. F.; Peng, Q. M.; Liu, M. H. Self-assembled luminescent quantum dots to generate full-color and white circularly polarized light. *Angew. Chem., Int. Ed.* **2017**, *56*, 12174–12178.

[32] Zhou, Y. J.; Jie, K. C.; Zhao, R.; Huang, F. H. Supramolecular-macrocycle-based crystalline organic materials. *Adv. Mater.* **2020**, *32*, 1904824.

[33] Rekharsky, M. V.; Inoue, Y. Complexation thermodynamics of cyclodextrins. *Chem. Rev.* **1998**, *98*, 1875–1918.

[34] Yoshizawa, M.; Kusukawa, T.; Kawano, M.; Ohhara, T.; Tanaka, I.; Kurihara, K.; Niimura, N.; Fujita, M. Endohedral clusterization of ten

water molecules into a “molecular ice” within the hydrophobic pocket of a self-assembled cage. *J. Am. Chem. Soc.* **2005**, *127*, 2798–2799.
[35] Trembleau, L.; Rebek, J. Helical conformation of alkanes in a hydrophobic cavitand. *Science* **2003**, *301*, 1219–1220.
[36] Dong, S. Y.; Zheng, B.; Wang, F.; Huang, F. H. Supramolecular polymers constructed from macrocycle-based host-guest molecular recognition motifs. *Acc. Chem. Res.* **2014**, *47*, 1982–1994.
[37] Li, Z. Y.; Zhang, Y. Y.; Zhang, C. W.; Chen, L. J.; Wang, C.; Tan, H. W.; Yu, Y. H.; Li, X. P.; Yang, H. B. Cross-linked supramolecular polymer gels constructed from discrete multi-pillar[5]arene metallacycles and their multiple stimuli-responsive behavior. *J. Am. Chem. Soc.* **2014**, *136*, 8577–8589.
[38] Chen, J. S.; Peng, Q. Y.; Peng, X. W.; Zhang, H.; Zeng, H. B. Probing and manipulating noncovalent interactions in functional polymeric systems. *Chem. Rev.* **2022**, *122*, 14594–14678.
[39] Lee, S.; Vo, T.; Glotzer, S. C. Entropy compartmentalization stabilizes open host-guest colloidal clathrates. *Nat. Chem.* **2023**, *15*, 905–912.
[40] Zhu, G. L.; Xu, Z. Y.; Yan, L. T. Entropy at bio-nano interfaces. *Nano Lett.* **2020**, *20*, 5616–5624.
[41] Frederick, K. K.; Marlow, M. S.; Valentine, K. G.; Wand, A. J. Conformational entropy in molecular recognition by proteins. *Nature* **2007**, *448*, 325–329.
[42] Zeno, W. F.; Thatte, A. S.; Wang, L. P.; Snead, W. T.; Lafer, E. M.; Stachowiak, J. C. Molecular mechanisms of membrane curvature sensing by a disordered protein. *J. Am. Chem. Soc.* **2019**, *141*, 10361–10371.
[43] Dai, X. B.; Chen, P. Y.; Zhu, G. L.; Xu, Z. Y.; Zhang, X. H.; Yan, L. T. Entropy-mediated mechanomutable microstructures and mechanoresponsive thermal transport of nanoparticle self-assembly in block copolymers. *J. Phys. Chem. Lett.* **2019**, *10*, 7970–7979.
[44] Liu, M. Z.; Zheng, X. L.; Grebe, V.; Pine, D. J.; Weck, M. Tunable assembly of hybrid colloids induced by regioselective depletion. *Nat. Mater.* **2020**, *19*, 1354–1361.
[45] Peng, L.; Peng, H. R.; Wang, S.; Li, X. J.; Mo, J. Y.; Wang, X.; Tang, Y.; Che, R. C.; Wang, Z. K.; Li, W. et al. One-dimensionally oriented self-assembly of ordered mesoporous nanofibers featuring tailorable mesophases via kinetic control. *Nat. Commun.* **2023**, *14*, 8148.
[46] Peng, C.; Zhang, Y. B.; Zhang, Y. F.; Hu, Y. Y.; Che, Y. K.; Zhao, J. C. Highly fluorescent nanotubes with tunable diameter and wall thickness self-assembled from asymmetric perylene diimides. *Small* **2016**, *12*, 4363–4369.
[47] Boaz, H.; Rollefson, G. K. The quenching of fluorescence. *Deviations from the Stern-Volmer law. J. Am. Chem. Soc.* **1950**, *72*, 3435–3443.
[48] Keizer, J. Nonlinear fluorescence quenching and the origin of positive curvature in Stern-Volmer plots. *J. Am. Chem. Soc.* **1983**, *105*, 1494–1498.
[49] Mao, X. M.; Chen, Q.; Granick, S. Entropy favours open colloidal lattices. *Nat. Mater.* **2013**, *12*, 217–222.
[50] Zhao, K.; Bruinsma, R.; Mason, T. G. Entropic crystal-crystal transitions of Brownian squares. *Proc. Natl. Acad. Sci. USA* **2011**, *108*, 2684–2687.
[51] van Anders, G.; Klotsa, D.; Ahmed, N. K.; Engel, M.; Glotzer, S. C. Understanding shape entropy through local dense packing. *Proc. Natl. Acad. Sci. USA* **2014**, *111*, E4812–E4821.
[52] Wang, Z. G. *50th anniversary perspective*: Polymer conformation-a pedagogical review. *Macromolecules* **2017**, *50*, 9073–9114.

This is an open access article under the terms of the Creative Commons Attribution 4.0 International License (CC BY 4.0, https://creativecommons.org/licenses/by/4.0/).

© The Author(s) 2026. Published by Tsinghua University Press.